

First-principles study of the mode-1 fracture of Fe-TiX interfaces (X=C,N)

Travis E. Jones,* Matt A. Sauer, and Mark E. Eberhart

Molecular Theory Group, Colorado School of Mines, Golden, Colorado 80401, USA

(Received 29 February 2008; published 8 September 2008)

We compare the evolution of the charge density in mode-1 fracture with that in uniaxial separation of two model systems: coherent Fe-TiC and Fe-TiN interfaces. These charge densities were calculated using both band structure and cluster codes. The topology of charge density in the cluster calculations converged with that of the bulk within two coordination spheres. Furthermore, we found that the topology of initial and final states is independent of the applied strain. However, the topological evolution is strain dependent. While we observed one topological catastrophe in Fe-TiC, independent of strain, we saw two separate catastrophes under uniaxial separation of Fe-TiN and only one under mode-1 fracture. This behavior suggests that there is some kinetic control mediating fracture in these iron-ceramic interfaces.

DOI: 10.1103/PhysRevB.78.092104

PACS number(s): 62.20.mm

Brittle failure is an important phenomenon that is believed to be controlled by interactions at the tip of atomically sharp cracks.¹ In an effort to gain insight into fractures' atomic scale mechanism and ultimately limit its costly consequences, many investigators have turned to first-principles methods. However, due to symmetry breaking and complex crack tip reconstruction, quantitative calculations of even simple cleavage process are computationally intractable. Hence, rather than modeling fracture directly, most studies have been concerned with calculating pertinent thermodynamic parameters such as the ideal work of adhesion.² The kinetic aspects of fracture have been all but ignored, even though some have suggested that fracture may have a kinetic component and, if so, would be subjected to kinetic control.^{3,4} Our objective is to assess this possibility.

In this study we have modeled decohesion in two idealized systems: coherent Fe-TiC and Fe-TiN interfaces. Our goal is to determine how the charge redistribution accompanying fracture is influenced by chemistry and fracture path. What makes this approach unique is that the charge redistribution is described topologically, allowing us to identify topological transition states (TTSs) along the chosen fracture path. Once identified, we are able to apply the Hammond postulate and make rough estimates of the comparative energies of path- and chemistry-dependent transition states.

The Hammond postulate⁵ was first articulated in 1955 and became one of the most cited articles of the *Journal of the American Chemical Society* (over 3000 cites to date). Hammond proposed that for two similar reactions, the one in which the transition state comes earlier in the process will be the one preferred. This postulate is quite general and, in principle, can be applied to condensed phase phenomena. In 1982, Whitesides⁴ stressed that the conceptual framework of chemistry, particularly transition state theory and the Hammond postulate, may have applications in the study of deformation and fracture.

To exploit the Hammond postulate we appeal to Bader's⁶ topological theory of molecular structure, atoms in molecules. It is known from the Hohenberg-Kohn theorem that a system's ground-state properties are a consequence of its charge density, a scalar field denoted here as $\rho(\vec{r})$.⁷ Bader noted that the essence of a molecule's structure must be con-

tained within the topology of $\rho(\vec{r})$. The topology of a scalar field, in this case $\rho(\vec{r})$, is given in terms of its critical points (CPs), which are the zeros of the gradient of this field. There are four kinds of CPs in a three-dimensional space: a local minimum, a local maximum, and two kinds of saddle points. These CPs are denoted by an index, which is the number of positive curvatures minus the number of negative curvatures. For example, a minimum CP has positive curvature in three orthogonal directions; therefore, it is called a (3,3) CP. The first number is simply the number of dimensions of the space, and the second number is the net number of positive curvatures. A maximum is denoted by (3,-3), since all three curvatures are negative. A saddle point with two of the three curvatures negative is denoted (3,-1), while the other saddle point is a (3,1) CP.

Through extensive studies of molecules and crystals, Bader⁶ showed that it was possible to correlate topological properties of the charge density with elements of molecular structure and bonding. A maximum, a (3,-3) CP, is always found to coincide with the atomic nucleus, and so it is called an atom CP. But of greater importance, a bond path was shown to correlate with the ridge of maximum charge density connecting two nuclei such that the density along this path is a maximum with respect to any neighboring path. The existence of such a ridge is guaranteed by the presence of a (3,-1) CP between nuclei. As such, this critical point is often referred to as a bond CP. Other types of CPs have been correlated with other features of molecular structure. A (3,1) CP is required at the center of ring structures. Accordingly, this CP is designated a ring CP. Cage structures are characterized by a single (3,3) CP within the cage, and again, these CPs are given the descriptive name of cage CPs.

With a description of molecular structure in terms of the topology of $\rho(\vec{r})$, it is possible to represent fracture in terms of the topological evolution of $\rho(\vec{r})$. Those points where the topology of $\rho(\vec{r})$ changes, i.e., at catastrophes, will correspond to TTSs. By the Hammond postulate, the relative energy of these states can be assessed.

Calculations were performed with both VASP (Ref. 8) and Amsterdam density functional (ADF).⁹ We made use of the Perdew-Wang 91 generalized gradient corrections.¹⁰ The calculations consisted of two parts: (1) building clusters that

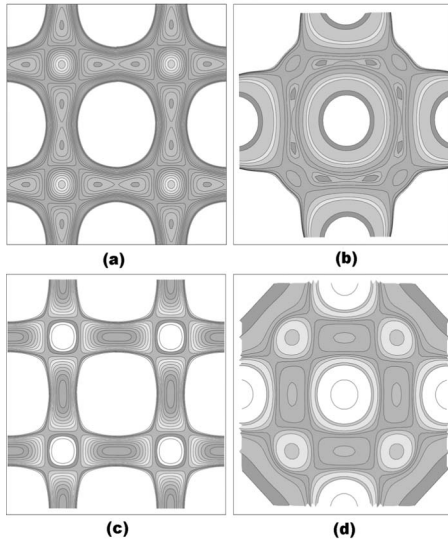


FIG. 1. Contour plots cutting across both the Fe-TiC [FLAPW (a) and ADF (b)] and Fe-TiN interfaces [FLAPW (c) and ADF (d)].

capture ground-state topology of the bulk material and (2) fracturing these clusters under tensile loading to observe how the topology evolves using TECPLOT.¹¹

Interfaces normally form between the most stable free surfaces. Thus, we chose to study the Fe(110)-TiC(100) and Fe(110)-TiN(100) interfaces. The Freeman group supplied the ground-state charge density and atomic structures of the coherent interfaces, resulting from full-potential linearized augmented plane wave (FLAPW) calculations performed at varying interfacial separation distances.¹²

The atomic positions for the fully relaxed interfaces were used to generate clusters to determine the minimum size necessary to capture the correct topology. The electronic structure of 18 (nine for both Fe-TiC and Fe-TiN) different clusters was calculated. All were centered about the Fe- X ($X=C,N$) bond, as the interface Fe has a strong site preference.¹² The number of coordination spheres ranged from 1 to 3 and the number of layers from 2 to 4.

Previously we have seen that, unlike energy, topology converges rapidly with cluster size. In this study the topology of both interfaces converged at two coordination spheres and four layers, two Fe and two Ti X . Figure 1 shows a contour plot of the charge density in a plane bisecting the Fe- X bond in both the FLAPW and ADF charge densities. Inspection of this figure reveals that the topology from both methods is identical. In particular both systems have a cage point (bond point) between Fe-Ti (Fe- X). Another interesting feature in both systems is the presence of second-neighbor bonds between Fe atoms near the interface. This topology is not observed in pure bcc metals except near free surfaces. While the two interfaces share some topological features, there are also subtle differences. The Fe-TiC interface has a cage-ring-cage moiety in the plane, while Fe-TiN has only a cage point, both of which are marked in Fig. 1. This topological convergence leads us to conclude that the general interactions between the metal and ceramic are controlled by local interactions.

The topological evolutions of Fe-TiC under mode-1 frac-

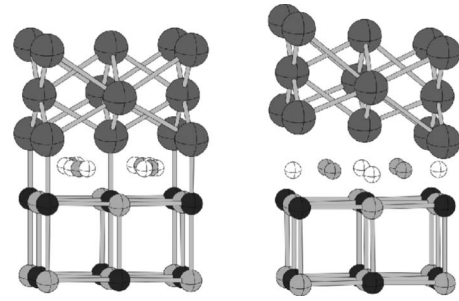


FIG. 2. Initial and final topologies in the Fe-TiC interface. Here the iron atoms are above the plane while the titanium (gray) and carbon (black) are below. Cage CPs are the small spheres shown in white and ring CPs in gray. The final topology is independent of fracture mode, and that shown for Fe-TiC is identical to Fe-TiN.

ture and uniaxial separation are similar. In both cases, as the strain is increased, the cage-ring-cage moiety begins to separate. The cage CPs inside the material approach the Fe-Ti cage CP. Simultaneously (in the cluster) the cage CPs near the edge are pulled toward the vacuum region. As the strain is increased further, a series of catastrophes take place. Figure 2 shows the result. Here the cage CPs in the bulk material, and those in the interior of the cluster, have coalesced with the Fe-Ti cage CP, while the cage CPs near the edge of the cluster have moved into the vacuum region. The resultant topology is identical in both cases. A single ring CP is left in place of the cage-ring-cage, while the Fe-Ti cage point remains unchanged.

Mode-1 fracture of Fe-TiN, however, does not elicit a response analogous to what is observed in uniaxial separation. As this interface is separated rigidly, the Fe-Ti cage CP is transformed into a bond CP. It is not until the interfacial separation reaches 5 Å that the single cage CP is broken into its substituent cage-ring-cage moiety (like that found in Fe-TiC). This topology is unstable and immediately relaxes to the fully separated topology shown in Fig. 2. This can be thought of as a three-step process: (1) form Fe-Ti bond CP, (2) form cage-ring-cage moiety, and (3) relax to separated topology. Under mode-1 strain, however, the first step is not observed; the interface relaxes to its separated topology under a small perturbation. While the topological evolution in Fe-TiN under mode-1 strain is unlike that seen in the rigid separation, the final topology in the two cases is identical.

The differences in topological evolution between mode-1 fracture of the two interfaces can be linked through the Hammond postulate by associating the TTS with the juxtaposition of critical points, i.e., catastrophes. The nitride and carbide interfaces relax to identical separated topologies through the same mechanism. However, the strain required in the nitride is less than that required in the carbide. As such, the Fe-TiN TTS comes earlier than the Fe-TiC TTS, suggesting that the carbide is more adhesive under mode-1 fracture.

This application of the Hammond postulate to mode-1 fracture has led to the same conclusion as the work of adhesion calculated by Freeman. However, it simultaneously provides a mechanism for the differences in adhesion—the origins of the effect are a result of variations in bonding across the surface, and it is the ultimate cause of these differences to which we now turn.

Consider the coordination around the central carbon atom in Fig. 2. It is bound to one Fe above, four Ti's in the plane, and one Ti below the plane. For the sake of clarity, we define a reference frame with the z axis as passing through the center of the Fe-C-Ti bonds. The plane containing C and four Ti atoms will be the xy plane, with the x and y axes being orthogonal to the lines connecting nearest-neighbor Ti atoms. With respect to this frame, the d_{xz} (d_{yz}) orbital on the Fe atom can mix with the p_x (p_y) of the central C atom. The same picture could be drawn for the Fe-TiN interface by substituting C with N.

In both cases (C and N) the symmetry of the charge density around this site is C_{4v} . Hence, the x and y directions are indistinguishable, making the p_x and p_y orbitals on the central atom degenerate. When the Fe d_{xz} and d_{yz} , which are also degenerate, mix out of phase with the p_x and p_y orbitals on the central atom, a degenerate pair of antibonding molecular orbitals (MOs) are formed, denoted as E. As a result, the charge density in the x and y directions is reduced. This can be used to explain the presence of the cage-ring-cage set of critical points seen in Fe-TiC and not in Fe-TiN. When C is the central atom, the degenerate pair is not occupied as there are only four electrons on C. As a result, the density in the xy plane along the x and y directions is a maximum, as seen in Fig. 1. However, in the case of Fe-TiN, the orbitals are partially occupied, resulting in a minimum in the density along the x and y directions in the xy plane. Thus, the cage-ring-cage CPs seen in Fe-TiC are transformed to a single cage CP in Fe-TiN. (This is in good agreement with Dudiy and Lundqvist's¹³ work on Co-TiC and Co-TiN interfaces. In this case, the difference in adhesion between the two interfaces was also accounted for by an increase in the amount of antibonding character in the nitride interface.) It is these orbitals that give rise to the difference in adhesion.

As a crack propagates down either interface, charge will be transferred between the bonds across the interface into the material on either side. This charge redistribution is permitted through the coupling of MOs by the perturbation acting on the interface, in this case, the strain. Under uniaxial separation, the strain and the strain gradient are both totally symmetric. As a result only orbitals of the same symmetry can couple. In the case of Fe-TiN, this is manifested as the separation of the single cage CP into the cage-ring-cage triplet coming late in the process. It can be seen as follows: The origin of the single cage CP lies with the highest occupied molecular orbital (HOMO), which reduces as E. Charge can only be transferred from this MO to an unoccupied MO of the same symmetry. However, there are no unoccupied MOs of E symmetry near the HOMO. Thus, charge is transferred from a near HOMO Fe-Ti antibonding orbital of B_2 symmetry to a low-lying unoccupied MO of B_2 symmetry. This results in the formation of a Fe-Ti bond CP. It is not until late in the process that the charge in the Fe-N antibonding MO can be transferred to another orbital of the same symmetry, allowing the cage-ring-cage to form. Thus, symmetric strain gives rise to two distinct TTSSs, as only MOs of the same symmetry can couple under such a strain.

If, however, the strain breaks all symmetry, as will be the case for mode-1 fracture, orbitals of any symmetry may couple. Under these conditions, the cage CP in the Fe-TiN

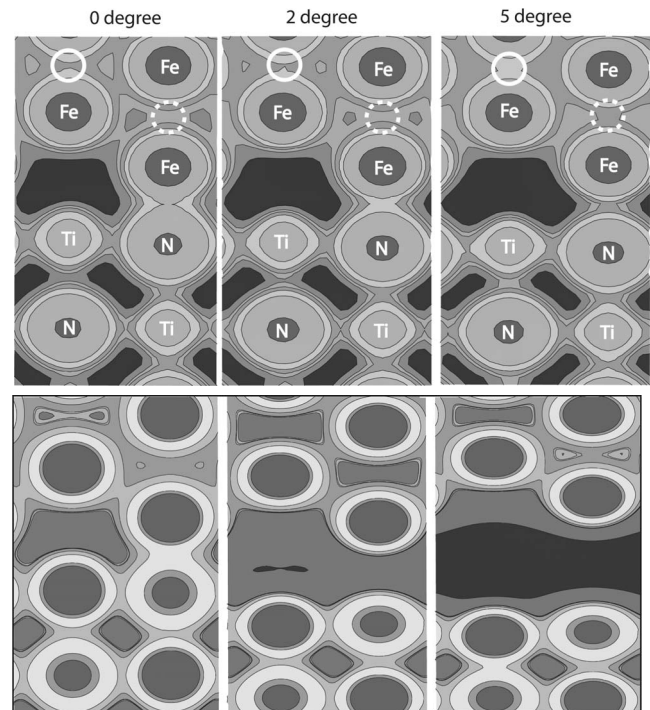


FIG. 3. Charge-density contour plots for mode-1 fracture (top) and rigid separation (bottom) of Fe-TiN. The density in the second-neighbor iron bonds, circled, increases under mode-1 fracture. However, under rigid separation the density is depleted during fracture.

interface separates immediately into the cage-ring-cage moiety. Here the HOMO can couple with the d_{z^2} orbitals on Fe. This coupling results in an increase in charge density between the second-neighbor Fe-Fe bonds at the interface during fracture. Figure 3 shows a set of contour plots wherein Fe-TiN is fractured under totally symmetric and mode-1 strains. The charge density between second-neighbor Fe atoms decreases during the early phases of uniaxial separation. It is not until the interface becomes free surface that the charge in the second-neighbor bond CP increases. This contrasts with mode-1 fracture. Here the charge in the second-neighbor Fe-Fe bond CP increases immediately, coincident with the separation of the single cage CP into the cage-ring-cage triplet. This bond strengthening tends to stabilize the TTS, making it occur earlier in the strain coordinate. Thus, the coupling under mode-1 strain allows the system to reach the TTS sooner than what is observed under uniaxial strain. While not shown, the same charge transfer mechanism is also seen in Fe-TiC, although it occurs at a slower rate with respect to strain.

In summary, employing qualitative transition state theory in conjunction with first-principles density-functional theory calculations and one-electron molecular-orbital theory has allowed us to formulate a chemical mechanism of fracture in coherent iron-ceramic interfaces. This approach can be employed to study the kinetics of fracture. In the model systems studied here we have shown that the kinetics of adhesion is mediated by the number of electrons in antibonding orbitals at the interface. While C does not fill antibonding orbitals, N

does. The result is that the Fe-TiC interface is more cohesive under mode-1 strain. This picture can easily be extended to other transition metals as well. Substituting Ti with V or Nb in Fe-TiC, for instance, will give results like those seen in Fe-TiN.

These results suggest that in coherent Fe-TiX ($X=C,N$) interfaces, adhesion is controlled by both the thermodynamics and kinetics of fracture. While uniaxial separations capture the former, they offer little insight into the latter. A totally symmetric strain will not allow coupling that facilitates

charge transfer from the bonds across the interface to bonds in the material on either side of the interface as is evident in Fig. 3. In the coherent interfaces this charge transfer tends to alter the TTS and thereby alters the kinetic control of fracture. We are currently working to extend this approach to the total charge density, and spin densities,¹⁴ of semicoherent iron-ceramic interfaces.

We wish to acknowledge the support of the Office of Naval Research for funding this work.

*trjones@mines.edu

¹J. R. Rice and R. Thomson, *Philos. Mag. B* **29**, 73 (1974).

²R. Wu, A. J. Freeman, and G. B. Olson, *Science* **265**, 376 (1994).

³M. E. Eberhart, R. M. Lantanson, and K. H. Johnson, *Acta Metall.* **33**, 1769 (1985).

⁴G. M. Whiteside, *Atomistics of Fracture* (Plenum, New York, 1983), p. 337.

⁵G. S. Hammond, *J. Am. Chem. Soc.* **77**, 334 (1955).

⁶R. F. W. Bader, *Atoms in Molecules: A Quantum Theory* (Clarendon, Oxford, UK, 1990).

⁷P. Hohenberg and W. Kohn, *Phys. Rev.* **136**, B864 (1964).

⁸G. Kresse and J. Furthmuller, *Comput. Mater. Sci.* **6**, 15 (1996).

⁹G. te Velde, F. M. Bickelhaupt, S. J. A. van Gisbergen, C. Fonseca Guerra, E. J. Baerends, J. G. Snijders, and T. Ziegler, *J. Comput. Chem.* **22**, 931 (2001).

¹⁰J. P. Perdew, J. A. Chevary, S. H. Vosko, K. A. Jackson, M. R. Pederson, D. J. Singh, and C. Fiolhais, *Phys. Rev. B* **46**, 6671 (1992).

¹¹TECPLOT, Seattle, WA (<http://www.tecplot.com>).

¹²T. Shishidou, J. H. Lee, Y. J. Zhao, A. J. Freeman, and G. B. Olson, *J. Appl. Phys.* **93**, 6876 (2003).

¹³S. V. Dudiy and B. I. Lundqvist, *Phys. Rev. B* **64**, 045403 (2001).

¹⁴T. E. Jones, M. E. Eberhart, and D. P. Clougherty, *Phys. Rev. Lett.* **100**, 017208 (2008).